Flexible neural connectivity under constraints on total connection strength

Gabriel Koch Ocker[1*], Michael A. Buice[1, 2],

1 Allen Institute for Brain Science, Seattle, WA, USA
2 Department of Applied Mathematics, University of Washington, Seattle, WA, USA

* gabeo@alleninstitute.org

Abstract

Neural computation is determined by neuron dynamics and circuit connectivity. Uncertain and dynamic environments may require neural hardware to adapt to different computational tasks, each requiring different connectivity configurations. At the same time, connectivity is subject to a variety of constraints, placing limits on the possible computations a given neural circuit can perform. It is desirable that constraints permit the circuit to be flexible in the sense that it be capable of learning to perform many different computations, so that the circuit can adapt to or develop towards the demands of its environment. Here we examine the hypothesis that neural circuitry is organized such that physiological constraints permit the highest possible degree of computational flexibility, i.e. that they allow for the largest possible number of computational solutions available to the circuit. From this hypothesis, we develop models of the degree distributions of connectivity based on constraints on a neuron's total synaptic weight. To test these models, we examine reconstructions of the mushroom bodies from the first instar larva and the adult *Drosophila melanogaster*. We perform a Bayesian model comparison for two constraint models and a random wiring null model. Overall, we find that flexibility under a homeostatically fixed total synaptic weight describes Kenyon cell connectivity better than other models, suggesting a principle shaping the apparently random structure of Kenyon cell wiring. Furthermore, we find evidence that larval Kenyon cells are more flexible earlier in development, suggesting a mechanism whereby neural circuits begin as flexible system that develop into specialized computational circuits.

Author summary

The structure of neural circuits provides a backbone for circuit function. Physiological constraints restrict the possible circuit configurations, so that healthy neural circuits must satisfy demands of both their constraints and their computational tasks. A desirable property of neural circuits is that they be able to perform a variety of computations. Here we examine simple models of constraints on total synaptic weights, and calculate the number of configurations they allow: their computational flexibility. We propose probabilistic models of connectivity that weight the number of synaptic partners according to computational flexibility. High-throughput electron microscopic anatomical experiments have begun to yield detailed connectivity maps at the resolution of individual synapses. We test our hypothesis using recent wiring diagrams from a learning center, the mushroom body, in the brain of the fly *Drosophila melanogaster*. We compare constraints that fix or that bound a neuron's total connection strength, and compare them to a simple random wiring null model. Of these models, the fixed total connection strength matched the overall connectivity best in mushroom bodies from both larval and adult flies. We provide evidence that neural circuits are more flexible in early stages of development and lose this flexibility as they grow towards specialized function.

Introduction

The connectivity of neural circuits, together with neurons' intrinsic dynamics, determines their computation. Neural computations can shape, and in turn be shaped by, experience-dependent plasticity. Many studies have examined the

hypothesis that neural circuits might be optimal for sensory inference or metabolically efficient encoding(e.g., [1–5]). Random connectivity in cerebellar and cerebral cortices may form high-dimensional representations to facilitate associative learning and linear readout [9–12] and the synaptic weight distributions of Purkinje cells and cortical pyramidal neurons are consistent with the perceptron model with optimal associative memory [13–16].

Neuronal connectivity is also homeostatically regulated and constrained by physiological limits. Minimizing the amount of wire used to connect neural circuits can predict the spatial layout of neural systems (e.g., [17–21]) and dendritic arborizations. [22, 23] The total strength of synaptic connections between two neurons is limited by the amount of receptor and neurotransmitter available and the size of the synapse [24]. Pyramidal neurons of the cortex and hippocampus undergo synaptic scaling, regulating their total excitatory [25–28] and inhibitory [29–33] synaptic input strengths to regulate postsynaptic activity levels [34]. In *Drosophila melanogaster*, growth from the first instar larva to the third instar larva is accompanied by a homeostatic regulation of mechanosensory receptive fields [35] and functional motor neuron outputs [36] and nociceptive projections [37]. In addition, changes in inputs to the central aCC neuron elicit structural modifications to its dendritic tree that homeostatically maintain input levels [38].

Despite these constraints, neural connectivity must enable computation. Learning, furthermore, requires changes in synaptic weight configurations. In simple neural network models, constraints define a space of possible synaptic weights (the "constraint space"; Fig. 1a, b gray regions), while the synaptic weights that perform a particular computation define another space (the "computation space"; Fig. 1a, b colored regions). The intersection of the constraint and computation spaces defines the allowed synaptic weights (the "solution space"). The size of the solution space is then bounded by the size of the constraint space and the size of the computation space. A large solution space can be beneficial to maintain performance if synaptic weights fluctuate, to enable fast learning, or to allow the circuit to learn a variety of tasks, i.e. to be flexible. While the computation space is circuit-dependent and may change with experience and environment, the constraint space reflects the underlying neurophysiology. We reasoned that in order for the constraints to interfere minimally with computation and, moreover, to facilitate as wide an array of learnable computations as possible, neural connectivity should have evolved to maximize the total number of configurations available under physiological constraints. That is, the circuit might have evolved to be flexible under constraints. Such flexibility would be beneficial to an organism by facilitating task switching or may be a crucial component of development, with circuits initially constructed for flexibility developing towards specialized computations due to interaction with the environment.

We formulate this idea through simple models of constraints on a neuron's total connectivity. We consider two constraints: a 1) bounded or 2) fixed total connection strength. These lead us to hypothesize probabilistic models for the number of synaptic partners to a neuron. We test these constraint models against each other and a simple random wiring null model using recently available electron microscopic wiring diagrams of an associative learning center in *Drosophila melanogaster*, the larval [39] and adult [40] mushroom bodies. A combinatorial code for odorants in the first mushroom body neurons, Kenyon cells (KCs), [41–43] forms a substrate for associative learning at output neurons [44, 45]. We found that overall, the fixed net weight model provided the best description for Kenyon cell connectivity, suggesting that flexibility under homeostatic weight regulation governs KC connectivity. The one exception we saw was the mature KCs of the larval mushroom body, which were better described by a binomial random wiring model. This suggests a developmental progression in the structure of random KC wiring in the larva.

Results

Measuring constraint flexibility

We begin with a simple example where a neuron has N units of synaptic weight, of size ΔJ, available. These could correspond, for example, to individual receptors or vesicles. It can assign these synaptic weight units to its K partners (presynaptic partners as in Fig. 1c for receptors, or postsynaptic partners for vesicles). We will also call the number of synaptic partners the degree or connectivity degree. To measure how flexible or tight the constraint of having N synaptic weight units with K partners is, we can count the possible connectivity configurations. For $N = 4$ and two connections, there are six possible configurations. With three connections, there are four possible

configurations. Thus with the constraint of $N = 4$, two connections are more flexible than three since there are more ways to satisfy the constraint. Since the constraint treats all synaptic partners symmetrically, the number of possible configurations is given by the binomial coefficient "N choose K". For different numbers of synaptic weight units N, there are different maximally flexible degrees K (Fig. 1d).

Synaptic weights can be made up of many small units of strength, corresponding to (for example) individual receptors or vesicles. So, we will model individual synaptic weights as continuous variables. Throughout, we will use "synaptic weight" and "connection strength" interchangeably to refer to the total strength of projections from one neuron to another.

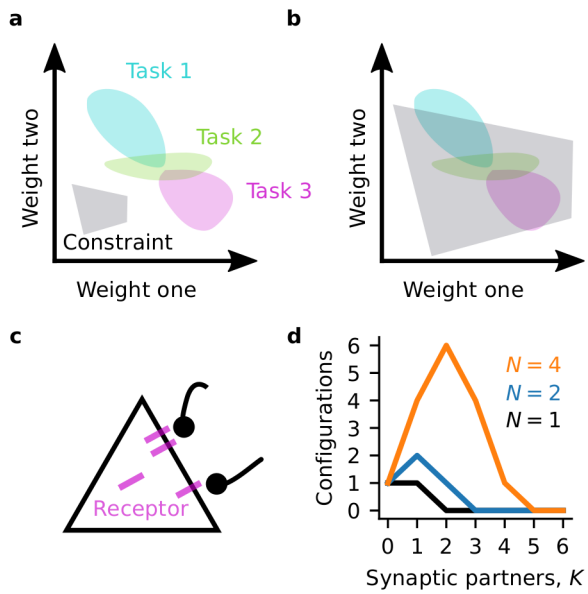

Fig 1. Constraints on synaptic connectivity. (**a**) Synaptic weights occupy a K-dimensional space. K is the number of synaptic partners. The solution spaces for computational tasks are subspaces of the synaptic weight space, with dimension up to K. Constraints also define subspaces with dimension up to K. A tight constraint defines a small subspace with low potential overlap with computational solution spaces. (**b**) A loose constraint defines a large subspace, with greater potential overlap with computational solution spaces. (**c**) A neuron that has $N = 4$ units of synaptic weight (here, receptors) to distribute amongst two synaptic partners and a pool of unused synaptic weight. (**d**) Number of possible connectivity configurations for different values of K and N (given by the binomial coefficient).

Degree distributions from constraints on net synaptic weights

We consider a simple model of synaptic interactions where a neuron has K synaptic partners and the strength of projection i is J_i. The first constraint we consider is an upper bound on the total connection strength:

$$\sum_{i=1}^{K} J_i \leq \bar{J} \tag{1}$$

This bound could be interpreted multiple ways, for example as a presynaptic limit due to the number of vesicles currently available before more are manufactured or a postsynaptic limit due to the amount of dendritic tree available for synaptic inputs. The value of this parameter, $\bar{J}$, could be set by metabolic or resource constraints.

With K synaptic partners, the constraint (1) defines a volume in K dimensions. For a neuron with two synaptic partners, this is the portion of the plane bounded by the axes and a line that stretches between them (Fig. 2a). For

three synaptic partners, the weights live in three-dimensional space and are constrained to lie in the volume under an equilateral triangle (Fig. 2b). (It is equilateral because its vertices are defined by the configurations where one connection uses the total weight, $\bar{J}$.) In general, for K synaptic partners the synaptic weights live in the volume under a $K-1$ dimensional simplex in K-dimensional synaptic weight space. The (Lebesgue or Hausdorff) measure of that volume is

$$V(K, \bar{J}) = \frac{\bar{J}^K}{K!} \tag{2}$$

This naturally extends the counting model of Fig. 1c, d to the case of a large pool of synaptic resources (Methods: Measuring synaptic weight configuration spaces) and measures the size of the space of allowed circuit configurations under the constraint of Eq. 1). The volume under the simplex increases with the max weight $\bar{J}$, but for fixed $\bar{J} \geq 2$ it is maximized at $K \geq 1$ (Fig. 1c).

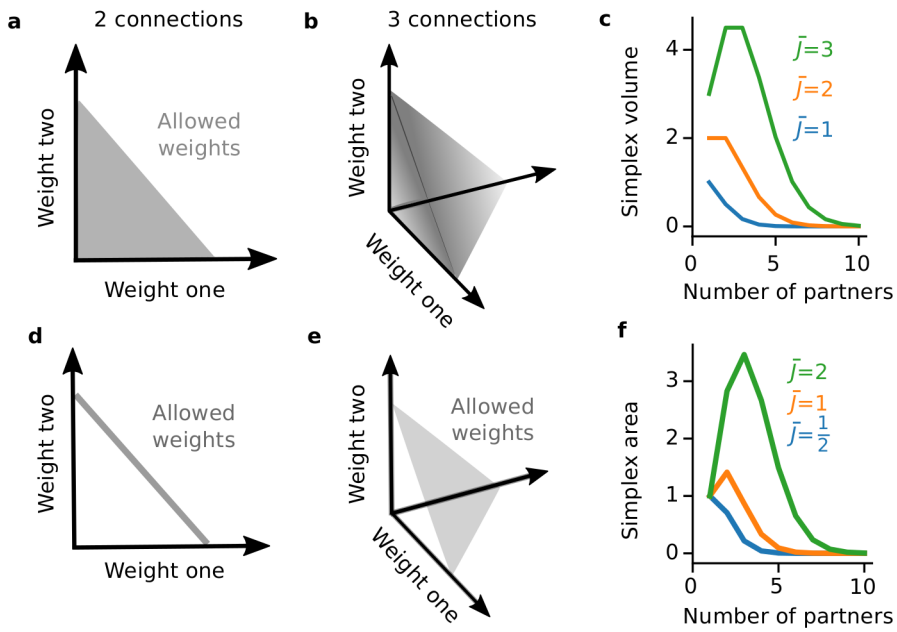

Fig 2. Constraints on total synaptic weights. (**a-c**) An upper bound on the total synaptic weight. (**d-f**) A fixed total synaptic weight. (**a**) For two inputs with a total synaptic weight of at most $\bar{J}$, the synaptic weights must live in the area under a line segment from $(0, \bar{J})$ to $(\bar{J}, 0)$ (a regular 1-simplex). (**b**) For three inputs, the synaptic weights must live in the volume under a regular two-simplex. (**c**) Volume of the $K-1$ simplex as a function of the number of presynaptic partners, K, for different maximal net weights $\bar{J}$. (**d**) For two inputs with a total synaptic weight fixed at $\bar{J}$, the synaptic weight configurations must be on the line segment from $(0, \bar{J})$ to $(\bar{J}, 0)$. (**e**) The solution space for the fixed net weight constraint with three inputs is an equilateral planar triangle (a regular 2-simplex). (**f**) Surface area of the regular $K-1$ simplex as a function of the number of presynaptic partners, K, for different net synaptic weights $\bar{J}$.

Under our hypothesis of flexible computation given a constraint, there should be a pressure on circuit structure that favors a large number of allowed synaptic weight configurations. As described above, for a fixed amount of synaptic resources, i.e. $\bar{J}$ fixed, the number of such configurations depends on the neuron's connectivity degree, K. We model this pressure by stipulating that the probability of having K synaptic partners given resource limits $\bar{J}$ is proportional to the number of configurations, i.e. the volume of the weight space with K partners. Hence, for the bounded net synaptic weight:

$$p_V(K|\bar{J}) = \frac{V(K, \bar{J})}{Z_V(\bar{J})} \tag{3}$$

where the subscript V marks the probability distribution as proportional to the simplex's volume and the normalization constant, Z_V, ensures that the probability distribution sums to 1:

$$Z_V(\bar{J}) = \sum_{K=1}^{\infty} V(K, \bar{J}) \tag{4}$$

This normalization constant can be computed exactly to reveal a zero-truncated Poisson distribution:

$$p_V(K|\bar{J}) = \frac{\bar{J}^K}{\left(\exp(\bar{J}) - 1\right) K!} \tag{5}$$

Note that this is a prediction for the number of synaptic partners to a neuron (its degree), not for its synaptic weights. The degree distribution is conditioned on the maximum total synaptic weight, as measured by the parameter $\bar{J}$.

In addition to facing resource constraints, neurons also homeostatically regulate their total input strengths [46]. Motivated by this homeostatic synaptic scaling, the next constraint we consider holds the total synaptic weight fixed at $\bar{J}$:

$$\sum_i J_i = \bar{J} \tag{6}$$

This constraint defines the surface of the same simplices discussed above (Fig. 2d, e) and their surface area measures the space of allowed configurations. We can compute that surface area by varying the volume (Eq. 1) along the normal vector from the origin to the simplex's centroid, $\left(\bar{J}/K\right)\vec{1}$ and normalizing by the length of that vector:

$$A(K, \bar{J}) = \frac{\bar{J}^{K-1}\sqrt{K}}{(K-1)!} \tag{7}$$

Like the simplex's volume, the surface area increases with the total synaptic weight $\bar{J}$ but for $\bar{J} \gtrapprox 0.7$ it has a maximum at $K \geq 1$ (Fig. 1f). We will also examine the size of this constraint as a model for conditional degree distributions:

$$p_A(K|\bar{J}) = \frac{A(K, \bar{J})}{Z_A(\bar{J})} \tag{8}$$

where p_A denotes the probability proportional to the simplex's surface area and the normalization constant is

$$Z_A(\bar{J}) = \sum_{K=1}^{\infty} \frac{\bar{J}^{K-1}\sqrt{K}}{(K-1)!} \tag{9}$$

In contrast to the bounded net weight model (Eq. 5), we are not aware of an exact solution for Z_A. When required, we will either approximate it by truncating at large K or bound it (Methods: Fixed net weight model).

Testing degree distribution models

To test these models, Eqs. 5 and 8, requires joint measurements of neurons' total synaptic weight and number of synaptic partners. One type of data with measurements reflecting both of these are dense electron micrographic (EM) reconstructions with synaptic resolution, where (in a tissue volume of sufficient size) all of a neuron's synaptic partners can be identified, and the size or number of synapses provide indirect measurements of the connection strength.

We used dense EM reconstructions of the mushroom bodies of the first instar larval *D. melanogaster* [39] and the alpha lobe of the adult [40]. The mushroom bodies are a center of associative learning and memory in the fly and other insects [44, 47]. Kenyon cells (KCs) are the first layer of processing the mushroom bodies, receiving input from sensory projection neurons and projecting to the mushroom body output neurons (as well as connecting recurrently to each other on their axons, and receiving inhibitory and modulatory inputs) [39, 40]. Olfactory inputs onto KCs are apparently random, with little dependence on space or correlation in numbers of partners [39, 41, 42, 48]. The reconstruction of the first instar larval mushroom body includes all pre- and postsynaptic partners of the Kenyon cells (KCs) [39]. The alpha lobe of the adult mushroom body is a structure defined by KC axons, and this data thus does not include inputs onto KC dendrites [40].

KCs can be morphologically classified by their age. In the first instar larva, mature KCs have dendrites that form claws around projection neuron axons. Young KCs do not have claws, and single-claw KCs are older than multi-claw KCs [39]. The adult's alpha lobe is defined by axons of KCs; that reconstruction does not include inputs onto the alpha lobe KCs' dendrites. The age of adult KCs can also be classified morphologically. KCs of the alpha prime lobe are born before KCs of the alpha lobe, and in the alpha lobe posterior KCs are born before surface KCs, which are in turn born before core KCs [49, 50]. We will examine the connectivity of these different KC classes separately.

These published EM data measured synapse counts. The relationship between synapse size and strength has been studied extensively in hippocampal pyramidal neurons, where synapse size and synapse strength are highly correlated [51–55]; we are not aware of measurements relating synapse count and physiological connection strength in Kenyon cells. To model this uncertainty we assumed that the total number of synapses onto a neuron, $\bar{S}$, is proportional to the physiological total connection strength constraint:

$$\bar{J} = \alpha \bar{S} \tag{10}$$

where α is the unknown constant relating the synapse count and the net synaptic weight. This assumption introduces α as an additional parameter in our degree distribution models, Eqs. 5 and 8, so that each neuron's degree is conditioned on two things: the unknown parameter α and that neuron's number of synapses $\bar{S}$.

In addition to the two constraint-inspired models of Eqs. 5 and 8, we also examined a simple random wiring null model where the number of partners follows a zero-truncated binomial distribution:

$$p_B(K|N, q) = \binom{N}{K} \frac{q^K (1-q)^{N-K}}{1-(1-q)^N} \tag{11}$$

This binomial wiring model assumes that each possible synaptic partner to a Kenyon cell has a fixed probability of making a connection, and that whether or not different potential partners actually connect are independent. In this binomial wiring model, each neuron's degree is conditioned on two things: N (the number of potential synaptic partners) and q (the connection probability). We used anatomical measurements for N (Methods: Zero-truncated binomial model) and took q as an unknown parameter for this model.

Explaining Kenyon cell input connectivity

We first examined the connectivity onto KCs, starting with the first instar larva [39]. We excluded inputs from the inhibitory APL neuron and the modulatory dopaminergic, octopaminergic, and interneurons (but obtained similar results when including them). As in previous studies, we used only reliable multi-synapse connections (but obtained similar results when including single-synapse connections) [39, 40]. We observed a wide range of numbers of presynaptic partners to KCs, with very different degree distributions for young and clawed KCs (Fig. 3a histograms).

As a first test, we examined the maximum likelihood marginal degree distributions. That is, we computed the maximum likelihood value of α to obtain the conditional degree distribution $p(K|\hat{\alpha}, \bar{S})$ and then marginalized out the observed distribution of $\bar{S}$ to compute $p(K|\hat{\alpha})$ (Fig. 3a, solid lines). For the binomial model we computed the maximum likelihood value of the connection probability q (Fig. 3a, dashed lines). For the young KCs, the fixed net weight model appeared to match the marginal degree distributions better than the binomial wiring model (Fig. 3a).

To better measure and compare how well those models explain KC connectivity we will compute their evidence, marginalizing over the unknown parameter α. For the fixed net weight, for example,

$$p_A(K|\bar{S}) = \int_0^\infty d\alpha \, p(\alpha) \prod_i p_A(K_i|\alpha, \bar{S}_i) \tag{12}$$

where i indexes KCs and $p(\alpha)$ is a prior distribution for α. We have a corresponding integration over α to find the model evidence of the bounded net weight model, and for the binomial wiring model an integration over the unknown connection probability q. We computed the Laplace approximations to these model evidences (Methods:

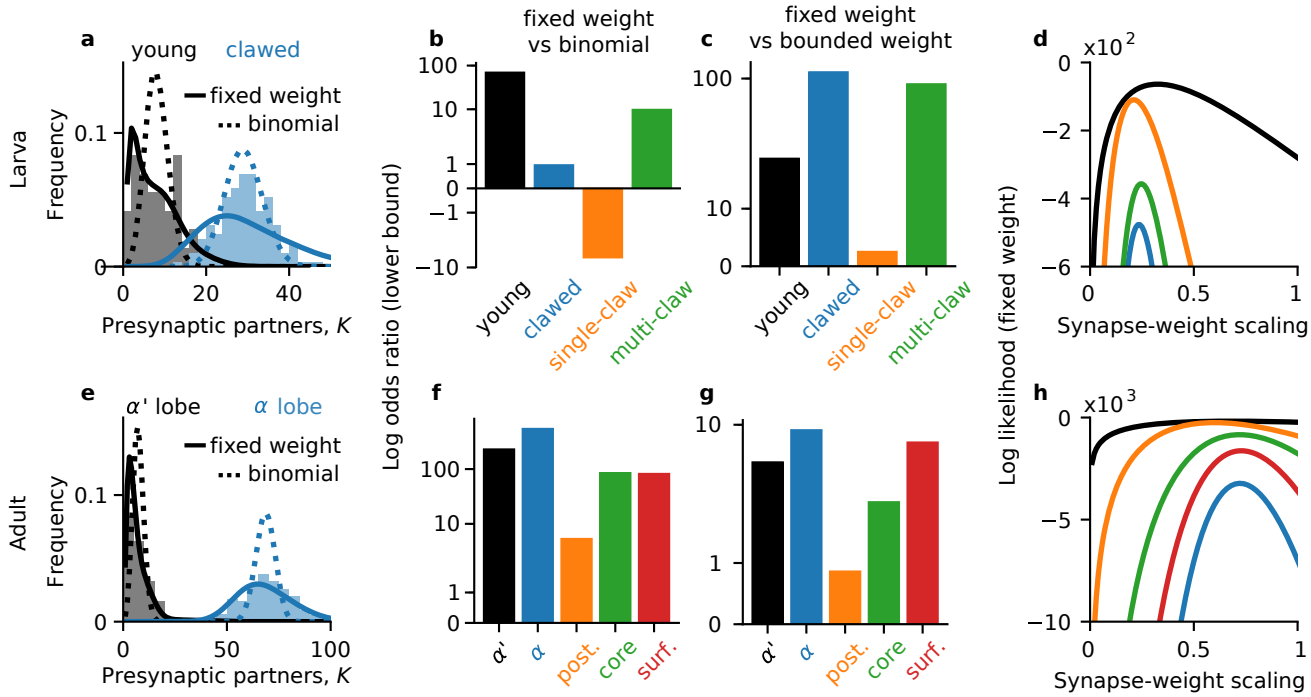

Fig 3. Kenyon cell input degree distributions. (**a**) Distribution of number of presynaptic partners for larval KCs. Shaded histograms: empirical distribution. Solid lines: the marginal simplex area distribution at the maximum likelihood value of α, after integrating out the number of synapses $\bar{S}$ against its empirical distribution. Dotted lines: the maximum likelihood binomial distribution. (**b**) Lower bound for the log evidence ratio (log odds) for the fixed net weight and binomial wiring models. Positive numbers favor the fixed weight model. Evidences computed by a Laplace approximation of the marginalization over the parameters. (**c**) Lower bound for the log odds for the fixed net weight and bounded net weight models; positive numbers favor the fixed weight model. (**d**) Log likelihood of the fixed net weight model as a function of the scaling between synapse counts and net synaptic weights. (**e-h**) Same as (**a-d**) but for adult alpha lobe KC axonal inputs.

Model comparison). Taking Eq. 12 as example, the Laplace approximation results from writing $p_A = \exp \ln p_A$ and Taylor expanding $\ln p_A$ in α around its maximum likelihood value. Truncating at second order then yields a tractable Gaussian integral over the unknown parameter.

Calculating the model evidence requires choosing a prior distribution for the unknown parameter. We first used a flat prior on non-negative values. Because the normalization constant for the fixed net weight model (Z_A, Eq. 9) was not analytically tractable, we computed upper and lower bounds for it. These bounds for Z_A then gave us bounds on the fixed net weight model's evidence (Methods: Fixed net weight model).

In the larva, the simplex area model outperformed the binomial model for both young and clawed KCs (Fig. 3c, log odds at least 70.46 and 0.97). We next asked whether this depended on the number of claws. The fixed net weight model outperformed the binomial wiring model for multi-claw KCs, but not single-claw KCs (Fig. 3b, log odds at least 9.92 for multi-claw KCs; Supp. Fig. 1b, log odds at most -1.57 for single-claw KCs). Within multi-claw KCs, the binomial model also outperformed the fixed weight model for two-claw KCs, but not for KCs with at least three claws (Supp. Fig. 1b). We found similar results comparing the bounded net weight model with binomial wiring (Supp. Fig. 1c). The fixed net weight model outperformed the bounded weight model for all KC types (Fig. 3c). For comparison with the adult data, we also examined KC-KC connectivity. We found similar results as for the full connectivity (Supp. Fig. 2a-d). Since single-claw KCs are more mature than multi-claw KCs [39], these results suggest that flexibility under a homeostatically fixed net weight governs KC input connectivity early in development, with other factors shaping connectivity after sensory and behavioral experience.

It is possible that these results depend on the prior distribution for α. We used the naively uninformative flat prior. Consider, however, a reparameterization of a degree distribution model as $p_A(K|\beta, \bar{S})$ where β is some monotonic function of α. A uniform prior on α can lead to a non-uniform prior on β—even though our ignorance about α should imply ignorance about β. The Jeffreys prior is invariant under monotone changes of variables, resolving this paradox [56]. Since the distribution obtained from the simplex volume is a zero-truncated Poisson distribution, we also checked the Jeffreys prior for the Poisson distribution (Methods: Model comparison) for α and q.

We obtained similar results with this Jeffreys prior. The fixed net weight model outperformed the bounded weight model for all KC types with the Poisson Jeffreys prior also (Supp. Fig. 1a; log odds of at least 1.34, 12.49, 1.37 and 9.86 for larval young, clawed, single- and multi-claw KCs respectively). The fixed net weight model and bounded net weight models outperformed the binomial model for young and multi-claw KCs (log odds at least 73.61 and 11.15 respectively), but not for single-claw or two-claw KCs (Supp. Fig. 1e, f; log odds at most -3.96 and -9.82 for single- and two-claw KCs).

We next asked whether the relationship between anatomical and physiological synaptic weights exhibited a similar developmental trajectory, with multi-claw KCs appearing more similar to young KCs. To this end, we examined the likelihood of the data under the fixed net weight model as a function of the scaling parameter α (Fig. 3d). We saw that that the maximum likelihood value of α, $\hat{\alpha}$, decreased with KC age (maximum likelihood values of α: 0.33, 0.25, and 0.21 for young, multi-claw, and single-claw KCs, respectively). The scaling for single- and two-claw KCs were similar ($\hat{\alpha}$ of 0.2 for two-claw KCs), while KCs with three or more claws had $\hat{\alpha} \geq 0.25$. Under the simple model of Eq. 10, these suggest that the translation of synapse counts into a physiologically regulated net synaptic weight becomes weaker during KC maturation. This could relate to the spatial concentration of synapses in claws of the dendrite.

As in the larva, adult KCs exhibited a range of in-degrees. KCs in the alpha prime lobe receive fewer axonal inputs than KCs in the alpha lobe (Fig. 3e). As before, we computed the maximum likelihood marginal degree distributions, and saw that the binomial model appeared much worse than the fixed net weight model (Fig. 3e solid vs dashed lines). This observation was born out by the model evidence.

In the adult, the fixed net model explained the in-degree distribution of every KC type better than the binomial model (Fig. 3f; log odds at least 232.57, 551.5, 5.36, 85.82, and 83.02 for alpha prime, all alpha lobe, posterior, core and surface KCs respectively). The fixed net weight model also explained the in-degree distributions better than the bounded weight model (Fig. 3f; log odds at least 4.59, 9.0, 0.87, 2.0, and 6.96 for alpha prime, all alpha lobe, posterior, core and surface KCs respectively). The upper bounds for the log odds of the fixed net weight distribution were close to the lower bounds for the adult KCs (Supp. Fig. 3a, b). We found similar results using the Poisson Jeffreys prior for the unknown parameters α and q (Supp. Fig. 3d-f). In summary, the degree distributions of KC inputs in the adult alpha prime and alpha lobes are best described by flexibility under a homeostatically fixed net synaptic weight.

The scaling between synapse counts and synaptic weights varied by KC type in the adult (Fig. 3h). The maximum likelihood values for α were 0.68, 0.6, 0.73, and 0.72 for alpha prime, posterior, surface, and core KCs (ordered from approximately oldest to youngest). These suggest that in the alpha lobe, surface and core KCs have more input synaptic weight per synapse on average than posterior KCs. The log odds for the alpha prime KCs was much less sensitive to small values of α than the classes of alpha lobe KCs (Fig. 3h, black vs colored curves), suggesting a more heterogenous or flexible relationship between axonal input synapse counts and regulated synaptic weights in alpha prime KCs.

Explaining Kenyon cell output connectivity

We next turned to examine the output connectivity of the larva Kenyon cells (Fig. 4a). Here, the models of Eqs. 5, 8 predict total output connection strengths for KCs, rather than total input strengths. We compared these constraint models to the same simple binomial random wiring null model. Overall, we found similar results for the output connectivity degrees as for the inputs.

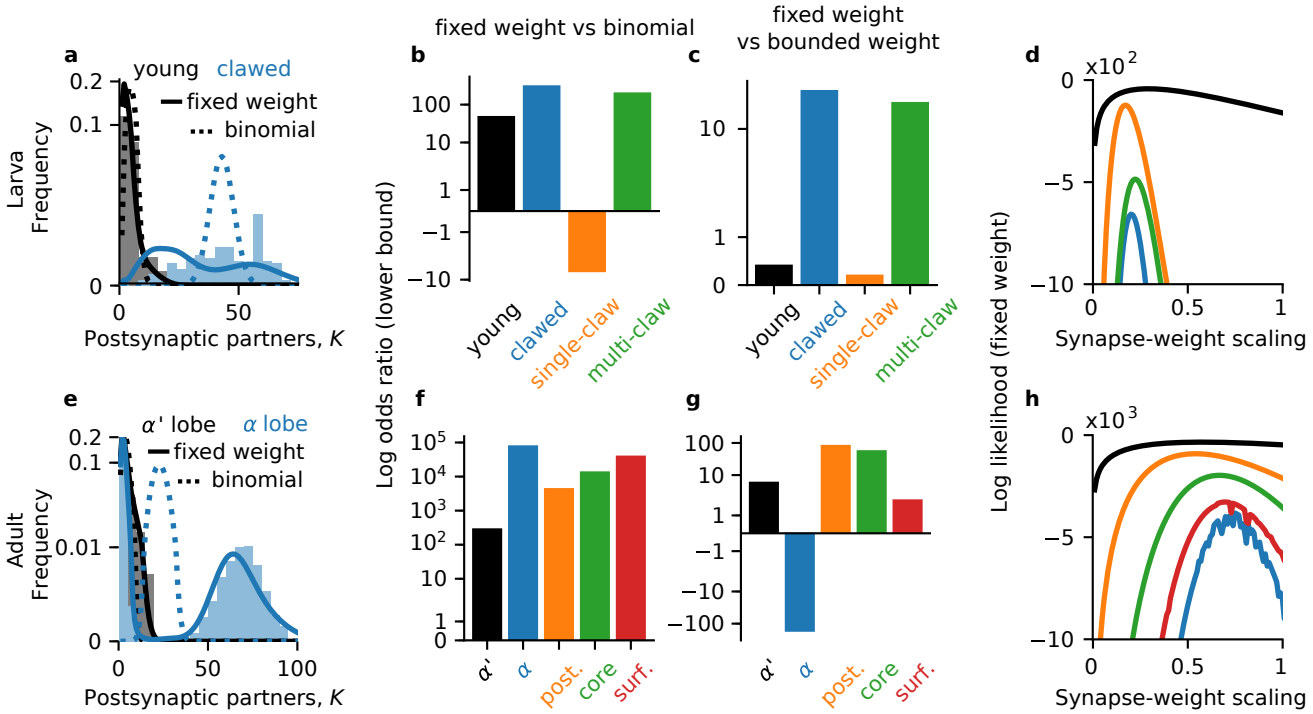

Fig 4. Kenyon cell output degree distributions. (**a**) Distribution of number of postsynaptic partners for larval KCs. Shaded histograms: empirical distribution. Solid lines: the marginal simplex area distribution at the maximum likelihood value of α, after integrating out the number of synapses $\bar{S}$ against its empirical distribution. Dotted lines: the maximum likelihood binomial distribution. (**b**) Lower bound for the log evidence ratio (log odds) for the fixed net weight and binomial wiring models. Positive numbers favor the fixed weight model. Evidences computed by a Laplace approximation of the marginalization over the parameters. (**c**) Lower bound for the log odds for the fixed net weight and bounded net weight models; positive numbers favor the fixed weight model. (**d**) Log likelihood of the fixed net weight model as a function of the scaling between synapse counts and net synaptic weights. (**e-h**) Same as (**a-d**) but for adult alpha lobe KC outputs.

For the larva KCs, the fixed net weight outperformed the binomial wiring for young and multi-claw KCs (log odds at least 48.17 and 201.8 respectively), but not for single- or two-claw KCs (log odds at most -0.78 and -0.50 respectively). For KCs with three or more claws, the log odds ratio for the fixed weight versus binomial wiring were at least 20.3 (Supp. Fig. 4b). The bounded net weight model outperformed the binomial wiring in the same cases - for young and clawed KCs, except for single- and two-claw KCs (Supp. Fig. 4c). The fixed net weight model described KC output degree distributions better than the bounded net weight for all types of KC in the larva (Fig. 4c, 4a). Under the Poisson Jeffreys prior, the only result that changed was that the bounded net weight was the best model for the young KC outputs (Supp. Fig. 4d-f). If we restrict the analysis to only KC-KC connectivity, then the fixed net weight model outperforms the binomial wiring and bounded net weight models for single-claw KCs (Supp. Fig. 2f, g), although not for two-claw KCs (not shown). Together, these results suggests that flexibility under a homeostatically fixed net synaptic weight regulates the input and output degree distributions of immature KCs, but that single- and two-claw KC degree distributions may be described better by a binomial wiring model.

As for the inputs, we found that the maximum likelihood values of α decreased with KC age, from 0.29 for young to 0.22 for multi-claw and 0.17 for single-claw KCs (Fig. 4d). The two-claw KCs exhibited a similar scaling as the single-claw KCs (0.17), while KCs with three or more claws had higher α values (0.24 for three- and four-claw KCs, 0.28 for five- and six-claw KCs). Similarly to for their inputs, these suggest that the relationship between net synapse counts and regulated net synaptic weights in the larva mushroom body may become weaker during KC maturation.

In the adult, Kenyon cells had heterogenous out-degrees, with alpha lobe KCs exhibiting a bimodal distribution (Fig. 4e). This bimodality was reflected in the out-degrees of posterior, core and surface KCs, rather than arising from one of those KC types (not shown). The fixed net weight models predicted adult KC out-degree distributions better than the binomial wiring model for all KC types (Fig. 4f), as did the bounded net weight model (Supp. Fig. 5f). The fixed net weight provided a better description for all the out-degree distributions of all types of adult KC than the bounded net weight, except when posterior core and surface KCs were all considered together (Fig. 4g). These results were consistent when using the Poisson Jeffreys prior for α and q (Supp. Fig. 5d-f). Together with the consistent results for adult KC input degrees (Fig. 3e-g), these suggest that flexibility under a fixed net synaptic weight governs KC connectivity in the alpha lobe of the mushroom body.

The scaling between the synapse count and net synaptic weight, α, exhibited similar patterns for adult KC outputs as for their inputs (Fig. 4h vs Fig. 3h). The maximum likelihood values of α were 0.58, 0.54, 0.7 and 0.67 for alpha prime, posterior, surface and core KCs respectively (in approximate developmental order). These suggest a divide with more mature KCs having more synaptic weight per synapse, on average, than younger KCs. Like for the inputs, the log likelihood for the alpha prime KCs was also much less sensitive to low values of α than the other KC types (Fig. 4h black vs colored curves), suggesting a more heterogenous or flexible relationship between axonal input synapse counts and regulated output synaptic weights similar to for the input synaptic weights (Fig. 4h black vs colored curves).

Optimally flexible connectivity

Above, we saw that KC connectivity degrees in the larval *Drosophila*, and KC axonal connectivity in the adult, were better described by a degree distribution proportional to the size of the space of allowed configurations under a fixed total synaptic weight. The most mature KCs of the larva (single-claw KCs), however, were best described by a binomial random wiring model. We next asked what circuits that directly maximize the size of those allowed synaptic weight spaces look like. For each constraint, we maximize the size of the allowed synaptic weight space to find the optimal degrees.

For the bounded net weight constraint (Eq. 1), this consists of maximizing the volume under the simplex (Eq. 2). This is equivalent to finding the mode of the zero-truncated Poisson distribution. We found (Methods: Optimal degrees: bounded net weight) an approximately linear relationship between the optimal degree and the maximum net connection strength:

$$K_V^* = \alpha \bar{S} - \frac{1}{2} + \mathcal{O}\left(1/K_V^*\right) \tag{13}$$

Under the fixed net weight constraint, we similarly found (Methods: Optimal degrees: fixed net weight) an approximately linear relationship between the optimal degree and the net connection strength:

$$K_A^* = \alpha \bar{S} + 2 + \mathcal{O}(1/K_A^*) \tag{14}$$

In both larval and adult KCs, we observed approximately linear relationships between the total number of synapses and number of partners for each KC type (Fig. 5). To quantify this, we computed the Pearson correlation between the number of synapses and number of partners for the different KC types. In the larval KCs, we found that less mature KCs better matched this linear relationship (Table 1: young > multi-claw > single-claw). The same was true for the adult KCs (Table 2: alpha prime > core > surface > posterior).

Table 1. Correlation of number of synapses and number partners in larval Kenyon cells

Cell type	Inputs	Outputs
Young	0.99	0.99
Multi-claw	0.77	0.86
Single-claw	0.67	0.8

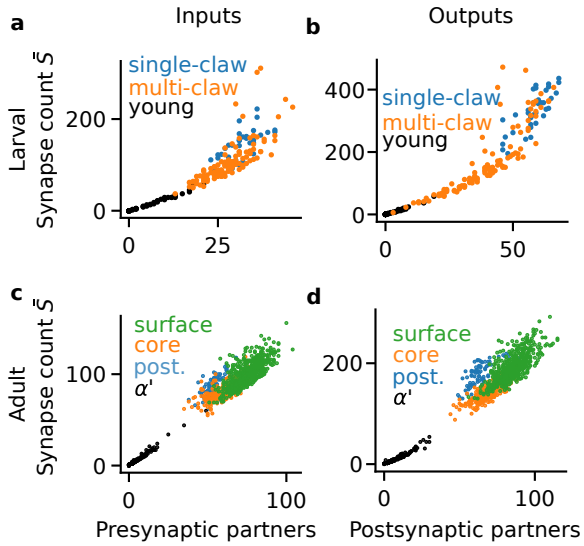

Fig 5. Relation between number of synaptic partners and synapse counts in *D. melanogaster* Kenyon cells. (**a**) Inputs to Kenyon cells (KCs) of the first instar larva. (**b**) Outputs of the first instar KCs. (**c**) Inputs to adult KCs in the α lobe. (**d**) Outputs of adult KCs in the α lobe.

Table 2. Correlation of number of synapses and number partners in adult alpha lobe Kenyon cells

Cell type	Inputs	Outputs
alpha prime	0.99	0.97
core	0.76	0.81
surface	0.74	0.74
posterior	0.69	0.69

Finally, we generalized this optimization to allow the constraints on total synaptic weights to explicitly depend on the number of inputs:

$$\sum_i J_i \leq \bar{J}K^p \text{ or } \sum_i J_i = \bar{J}K^p \tag{15}$$

for the bounded and fixed net weight constraints, respectively. This scaling of the summed synaptic weight corresponds to scaling the individual synaptic weights as K^{p-1}. If every synaptic weight has an order $1/K$ strength, the sum of the synaptic weights would be order 1 and $p = 0$. If every synaptic weight has an order 1 strength, the summed weight is order K and $p = 1$. If synaptic weights have balanced $(1/\sqrt{K})$ scaling [57], then the summed weight would have $p = 1/2$. Under this generalization of our constraint models, our Bayesian model comparisons still apply if we take the total synaptic weight to be proportional to the number of synapses $K^p\bar{J} = \alpha\bar{S}$ (instead of Eq. 10). That corresponds to the requirement that the scaling of synaptic weights with the number of inputs does not arise from scaling the number of synapses, but from other physiological mechanisms. This generalization still led to approximately linear relationships between the optimal degree and the total synaptic weight (Methods: Optimal degrees: bounded net weight and Optimal degrees: fixed net weight).

Discussion

We hypothesized that under a particular constraint, the probability of a neuron having K synaptic partners is proportional to the size of the space of allowed circuit configurations with K partners. The general idea of considering the space of allowed configurations can be traced back to Elizabeth Gardner's pioneering work examining the storage capacity of the perceptron for random input patterns [58]. In the limit of infinitely many connections and input patterns, the idea that a neuron performs associations leads to predictions for the distributions of synaptic weights [13–15, 59]. Here, in contrast, we examined the hypothesis that the size of the space of allowed configurations governs the distribution of the number of connections without defining a computational task. We examined constraints on the total strength of connections to (or from) a neuron, leaving the interaction of these with bounds on individual connection strengths for future work.

Measuring spaces of allowed circuit configurations

In measuring the size of configuration spaces, we assumed that the synaptic weight configuration can travel in a straight line between any two configurations, so that distances in the space of synaptic weights are Euclidean, measured by the root mean squared difference of their coordinates. If synaptic weights could not travel in a straight line, but rather each synapse would have to be potentiated or depressed separately, then we should instead use the 1-norm given by the sum of absolute differences. This changes the measure of the surface area of the simplex, replacing $\sqrt{K}$ by K in Eq. 7. This does not change the results of our analysis of KC input connectivity (Supp. Figs. 6, 7). For KC output connectivity, the bounded net weight was a better model than the fixed net weight, under the 1-norm for weight changes, for larval young KCs (Fig. 8) and adult surface KCs (Fig. 9).

Maximum entropy connectivity distributions

We modeled degree distributions as proportional to the size of the space of allowed K-dimensional synaptic weight configurations. For fixed K, the constraints we considered define spaces of allowed synaptic weight configurations, $\mathcal{S}_K$ (e.g. Fig. 2a,b,d,e). For the bounded net weight constraint, for example,

$$\mathcal{S}_K = \left\{ J \in \mathcal{R}_+^K \mid \sum_{i=1}^{K} J_i = \bar{J} \right\} \tag{16}$$

Given a fixed value of K, the maximum entropy distribution for the configurations J is the uniform distribution over $\mathcal{S}_K$. Take the total space of allowed configurations to be the union of the spaces of allowed configurations from $K = 1$ to some maximum value $K^{\max}$:

$$\mathcal{S} = \bigcup_{K=1}^{K^{\max}} \mathcal{S}_K \tag{17}$$

The maximum entropy distribution of synaptic configurations is again the uniform distribution over $\mathcal{S}$. If those $\mathcal{S}_K$ are disjoint, and we sample configurations according to that maximum entropy distribution, the probability that we obtain a configuration with a particular value of K will be proportional to the size of $\mathcal{S}_K$.

The definition of the total configuration space for synaptic weights, Eq. 17 is not the only possible one. The different subspaces $\mathcal{S}_K$ might not be disjoint. Furthermore, there could be multiple distinguished copies of each $\mathcal{S}_K$ in the total configuration space. More specific models of physiological constraints and synaptic pruning than those considered here might define different maximum entropy distributions for the synaptic configurations, implying different degree distributions. Finally, these models predict distributions of synaptic weights in addition to numbers of partners. Investigating specific maximum entropy connectivity models for synaptic weights and connectivity degrees presents, we believe, a promising direction for future work.

Flexible connectivity and circuit development

It is interesting to consider these results in the context of development. Computational flexibility should be desirable for an organism's fitness, allowing the organism to solve problems in a variety of environments. One mechanism of adaptability and flexibility is to build the nervous system out of computationally flexible units, that may over time adapt to specific computational roles. Our results are suggestive that this type of strategy may be at play in the development of mushroom body connectivity in the first instar *D. melanogaster* larva. The log odds for larval young KCs vastly favor the constraints models over the binomial model (Figs. 3c, 4c). The odds also approximately decreasingly favor the constraint model with KC maturity (Figs. 3, 4). In the adult, flexible connectivity under constraints on the net synaptic weight outperformed the binomial random wiring model most for the alpha prime KCs, and more for core than surface KCs (Figs. 3f, 4f, Supp. Figs. 3, 5). These suggest that flexibility under constraints might also reflect a developmental or experience-dependent progression in the alpha lobe KCs, but it remains a better explanation for their connectivity than binomial wiring even in the more mature KCs of the adult. The less mature KCs in the larva and adult also showed more linear relationships between their number of synapses and number of synaptic partners (Table 1), better matching the prediction of maximizing the space of allowed configurations under a constraint. Together, these results suggest that Kenyon cell connectivity is structured to be

flexible early in development, allowing many possible connectivity configurations to support specialization as the organism matures.

Materials and methods

Measuring synaptic weight configuration spaces

First, consider measuring the available configurations of synaptic weights when they can vary continuously. Consider the total synaptic weight, divided into K segments (Fig. 6). For one synaptic weight, the measure of the weight configurations is

$$\int_0^{\bar{J}} dJ_1 = \bar{J} \tag{18}$$

For two synaptic weights, the available configurations are measured by

$$\int_0^{\bar{J}} \int_{J_1}^{\bar{J}} dJ_2 \, dJ_1 = \frac{\bar{J}^2}{2} \tag{19}$$

and in general,

$$\int_0^{\bar{J}} \int_{J_1}^{\bar{J}} \int_{J_2}^{\bar{J}} \cdots \int_{J_{K-1}}^{\bar{J}} dJ_K \cdots dJ_3 \, dJ_2 \, dJ_1 = \frac{\bar{J}^K}{K!} \tag{20}$$

which is the volume under the simplex with vertex length $\bar{J}$.

Now consider synaptic weights that vary discretely by ΔJ, with $\bar{J} = N\Delta J$. How many ways can we assign N units of synaptic weight amongst K partners? For $K = 1$, this is N. For two synapses, this is

$$\sum_{n_1=1}^{N} \sum_{n_2=n_1}^{N} = \frac{N(N-1)}{2} \tag{21}$$

and in general the number of combinations of N units of synaptic weight in K connections is given by the binomial coefficient

$$\binom{N}{K} = \frac{N!}{K!\,(N-K)!} \tag{22}$$

For large N, the binomial coefficient is

$$\frac{N^K}{K!} \left(1 + \mathrm{O}\left(1/N\right)\right) \tag{23}$$

Now if we measure synaptic weights relative to ΔJ, this replaces $\bar{J}$ with $\bar{J}/\Delta J = N$ in the simplex's volume. So for large N, the volume under the simplex approximates the number of allowed configurations.

Similarly, the surface area of the simplex (Eq. 7) approximates the number of allowed configurations under the fixed net weight constraint (Eq. 6) if we discretize the synaptic weights. Note, however, that this surface area depends on the norm of the space of synaptic weight configurations (Methods)

Model comparison

Under equal prior likelihoods for two models X and Y, the posterior likelihood ratio between two models, X and Y is

$$\frac{p_X(K_i|\bar{S}_i)}{p_Y(K_i|\bar{S}_i)} = \frac{\int d\alpha \, \prod_i p_X(K_i|\bar{S}_i, \alpha) p(\alpha)}{\int d\alpha \, \prod_i p_Y(K_i|\bar{S}_i, \alpha) p(\alpha)} \tag{24}$$

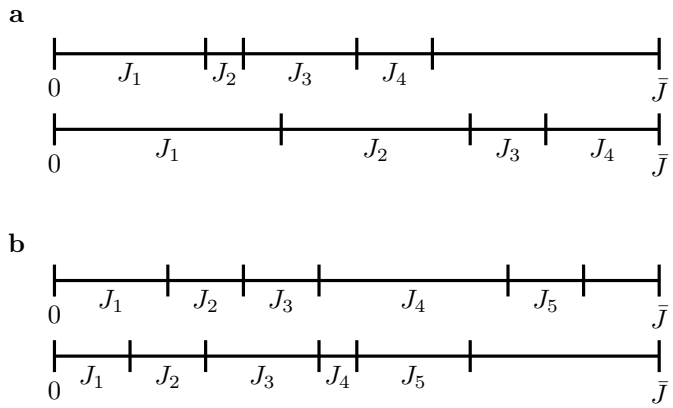

Fig 6. Synaptic weight configurations. a) Two example configurations of $K = 4$ synaptic weights with $J_1 + J_2 + J_3 + J_4 \leq \bar{J}$. **b)** Two examples of $K = 5$ synaptic weights with sum bounded by $\bar{J}$.

where i indexes data points. We consider the Laplace approximations for the posterior odds, obtained by expanding the log likelihood in α around the maximum likelihood value,

$$\hat{\alpha} = \arg\max_{\alpha} \prod_i p_X(K_i|\bar{S}_i, \alpha) \tag{25}$$

The Laplace approximation is:

$$\begin{aligned} \int d\alpha\, p(\alpha) \prod_i\, p_X(K_i|\bar{S}_i, \alpha) &= \int d\alpha\, p(\alpha) \prod_i\, \exp \ln p_X(K_i|\bar{S}_i, \alpha) \\ &\approx \int d\alpha\, p(\alpha) \prod_i\, p_X(K_i|\bar{S}_i, \hat{\alpha}) \exp \frac{-(\alpha - \hat{\alpha})^2}{2\sigma_i^2} \end{aligned} \tag{26}$$

where the integrals run over the allowed range for α and

$$\sigma_i^2 = -\left.\frac{\partial^2}{\partial \alpha^2} \ln p_X(K_i|\bar{S}_i, \alpha)\right|_{\hat{\alpha}} \tag{27}$$

Under a flat prior for non-negative α, the marginal likelihood is:

$$p_X(K_i|\bar{S}_i) \approx \left(\prod_i p_X(K_i|\bar{S}_i, \hat{\alpha})\right) \sqrt{\frac{\pi\sigma^2}{2}} \left(1 + \mathrm{Erf}\left(\frac{\hat{\alpha}}{\sqrt{2\sigma^2}}\right)\right) \tag{28}$$

where $1/\sigma^2 = \sum_i 1/\sigma_i^2$. The simplex volume distribution is a truncated Poisson; we might reasonably use the Jeffreys prior for the Poisson distribution, $p(\alpha) \propto 1/\sqrt{\alpha}$. In that case, the marginal likelihood is

$$p_X(K_i|\bar{S}_i) \approx \left(\prod_i p_X(K_i|\bar{S}_i, \hat{\alpha})\right) \frac{\pi\sqrt{\hat{\alpha}}}{2} \exp\left(-\frac{\hat{\alpha}^2}{4\sigma^2}\right) \left(\mathcal{I}_{-\frac{1}{4}}\left(\frac{\hat{\alpha}^2}{4\sigma^2}\right) + \mathcal{I}_{\frac{1}{4}}\left(\frac{\hat{\alpha}^2}{4\sigma^2}\right)\right) \tag{29}$$

where $\mathcal{I}_a$ is the modified Bessel function of the first kind. We will drop the indices on $K, \bar{S}$ in most of the remaining sections, reintroducing them where necessary.

Bounded net weight model

Under a bounded net weight, the degree distribution is:

$$p_V(K|\bar{S}, \alpha) = \frac{(\alpha\bar{S})^K}{Z_V(\bar{S}, \alpha)K!} \tag{30}$$

The normalization constant Z is

$$Z_V(\bar{S},\alpha) = \sum_{K=1}^{\infty} \frac{(\alpha\bar{S})^K}{K!} = \exp\left(\alpha\bar{S}\right) - 1 \tag{31}$$

so the simplex volume distribution is a zero-truncated Poisson distribution. We will make a Laplace approximation for the simplex volume distribution around $\hat{\alpha}$, leading to the posterior odds Eq. 28 (for a flat prior on non-negative α) or Eq. 29 (for the Poisson Jeffreys prior). To calculate the Laplace approximation for the posterior odds we need $\hat{\alpha}$ and σ^2. The derivatives of $\ln p_V$ can be calculated directly (again dropping indices over measurements),

$$\begin{aligned}
\frac{\partial}{\partial\alpha} \ln p_V(K|\bar{S},\alpha) &= \frac{K}{\alpha} + \bar{S}\left(\frac{1}{1-\exp\alpha\bar{S}} - 1\right) \\
\frac{\partial^2}{\partial\alpha^2} \ln p_V(K|\bar{S},\alpha) &= -\frac{K}{\alpha^2} + \left(\frac{\bar{S}}{2}\operatorname{Csch}\left(\frac{\alpha\bar{S}}{2}\right)\right)^2
\end{aligned} \tag{32}$$

So we have

$$\sigma^2 = \left(\sum_i \left(\frac{K_i}{\hat{\alpha}^2} - \left(\frac{\bar{S}_i}{2}\operatorname{Csch}\left(\frac{\hat{\alpha}\bar{S}_i}{2}\right)\right)^2\right)^{-1}\right)^{-1} \tag{33}$$

and the maximum likelihood solution for α satisfies

$$0 = \sum_i \frac{K_i}{\hat{\alpha}} - \frac{\bar{S}_i}{1-\exp\hat{\alpha}\bar{S}_i} \tag{34}$$

Fixed net weight model

Under the fixed net synaptic weight, our model is that the degree distribution is proportional to the surface area of the simplex:

$$p_A(K|\bar{S},\alpha) = \frac{1}{Z_A(\bar{S},\alpha)} \frac{(\alpha\bar{S})^{K-1}\sqrt{K}}{(K-1)!} \tag{35}$$

where

$$Z_A(\bar{S},\alpha) = \sum_{K=1}^{\infty} \frac{(\alpha\bar{S})^{K-1}\sqrt{K}}{(K-1)!} \tag{36}$$

To calculate $\hat{\alpha}$ and σ^2 we need the derivatives of $\ln p_A$.

$$\frac{\partial}{\partial\alpha} \ln p_A = \frac{\partial}{\partial\alpha} \ln A - \frac{\partial}{\partial\alpha} \ln Z \tag{37}$$

where

$$\frac{\partial}{\partial\alpha} \ln A = \frac{K-1}{\alpha} \tag{38}$$

and

$$\frac{\partial}{\partial\alpha} \ln Z = \frac{\frac{\partial}{\partial\alpha} Z}{Z} \tag{39}$$

We next approximate $\frac{\partial}{\partial\alpha} Z$.

$$\begin{aligned}
\frac{\partial}{\partial\alpha} Z &= \sum_{K=2}^{\infty} \frac{(\alpha\bar{S})^{K-2}}{(K-2)!}\sqrt{K}S \\
&= S\sum_{K=1}^{\infty} \frac{(\alpha\bar{S})^{K-1}}{(K-1)!}\sqrt{K+1} \\
&= S\sum_{K=1}^{\infty} \frac{(\alpha\bar{S})^{K-1}}{(K-1)!}\sqrt{K}\sqrt{1+\frac{1}{K}}
\end{aligned} \tag{40}$$

For $K \geq 1$, $\sqrt{1+1/K}$ is bounded above by $\sqrt{2}$ and below by 1. So,

$$SZ < \frac{\partial}{\partial\alpha} Z < \sqrt{2} SZ \tag{41}$$

Inserting these into the critical point equation for $\hat{\alpha}$ provides the bounds:

$$\frac{\sum_i (K_i - 1)}{\sqrt{2}\sum_i \bar{S}_i} < \hat{\alpha} < \frac{\sum_i (K_i - 1)}{\sum_i \bar{S}_i} \tag{42}$$

We will also need the curvature of $\ln p_A$ w.r.t. α at $\hat{\alpha}$:

$$\sigma^2 = -\frac{\partial^2}{\partial\alpha^2} \ln p_A \tag{43}$$

Similarly to the first derivative,

$$\frac{\partial^2}{\partial\alpha^2} \ln p_A = \frac{\partial^2}{\partial\alpha^2} \ln A - \frac{\partial^2}{\partial\alpha^2} \ln Z \tag{44}$$

where

$$\frac{\partial^2}{\partial\alpha^2} \ln A(K|\bar{S}, \alpha) = -\frac{(K-1)}{\alpha^2} \tag{45}$$

We use the identity

$$\frac{\partial^2}{\partial\alpha^2} \ln Z = \frac{\frac{\partial^2}{\partial\alpha^2} Z}{Z} - \frac{\left(\frac{\partial}{\partial\alpha} Z\right)^2}{Z^2} \tag{46}$$

The curvature of Z is

$$\begin{aligned} \frac{\partial^2}{\partial\alpha^2} Z &= S^2 \sum_{K=3}^{\infty} \frac{(\alpha\bar{S})^{K-3}}{(K-3)!} \sqrt{K} \\ &= S^2 \sum_{K=1}^{\infty} \frac{(\alpha\bar{S})^{K-1}}{(K-1)!} \sqrt{K+2} \\ &= S^2 \sum_{K=1}^{\infty} \frac{(\alpha\bar{S})^{K-1}}{(K-1)!} \sqrt{K} \sqrt{1 + \frac{2}{K}} \\ &\approx S^2 Z \end{aligned} \tag{47}$$

The final term $\sqrt{1+\frac{2}{K}}$ is bounded above by $\sqrt{3}$ and below by 1, so

$$S^2 Z < \frac{\partial^2}{\partial\alpha^2} Z < \sqrt{3} S^2 Z \tag{48}$$

Defining upper and lower bounds for $\frac{\partial^2}{\partial\alpha^2} \ln Z$ using the upper and lower bounds of the first and second terms in Eq. 46 yields:

$$-S^2 < \frac{\partial^2}{\partial\alpha^2} \ln Z < (\sqrt{3} - 1) S^2 \tag{49}$$

The upper bound for $\frac{\partial^2}{\partial\alpha^2} \ln Z$ provides an upper bound for σ^2, while neglecting Z provides a lower bound for σ^2 (since $Z \geq 1$ from Eq. 36, so that $\ln Z \geq 0$):

$$\frac{K-1}{\alpha^2} \leq \sigma^2 < \frac{K-1}{\alpha^2} + (\sqrt{3} - 1) S^2 \tag{50}$$

The posterior odds for the simplex area are:

$$\int d\alpha\, p(\alpha) \prod_i p_A(K_i|\bar{S}_i, \alpha) \approx \left(\prod_i p_A(K_i|\bar{S}_i, \hat{\alpha})\right) \int d\alpha\, p(\alpha) \exp\left(\frac{(\alpha - \hat{\alpha})^2}{2\sigma^2}\right) \tag{51}$$

where $\sigma^2 = 1/\sum_i 1/\sigma_i^2$. We use the upper and lower bounds for σ_i^2 to define upper and lower bounds, respectively, for the likelihood's variance:

$$\begin{aligned}\sigma_U^2 &= \left(\sum_i \left(\frac{(K_i-1)}{\hat{\alpha}^2} + \left(\sqrt{3}-1\right)\bar{S}_i^2\right)^{-1}\right)^{-1} \\ \sigma_L^2 &= \left(\sum_i \left(\frac{(K_i-1)}{\hat{\alpha}^2}\right)^{-1}\right)^{-1}\end{aligned} \tag{52}$$

We compute $\hat{\alpha}$ numerically by maximizing the likelihood, and compute $p_A(K_i|\bar{S}_i,\hat{\alpha})$ also numerically, estimating Z by ranging over $K = 1$ to $2\max_i \bar{S}_i$.

Bounds for the posterior odds of the fixed net weight model

The derivative of the posterior odds under the flat prior, Eq. 28, with respect to σ is proportional to

$$1 - \frac{\sqrt{2}\alpha \exp\left(-\frac{\alpha^2}{2\sigma^2}\right)}{\sqrt{\pi}s} + \mathrm{Erf}\left(\frac{\alpha}{\sqrt{2}\sigma}\right) \tag{53}$$

Since $\alpha > 0$ and $\sigma > 0$, the last term is bounded between 0 and 1. The middle term is of the form $x\exp(-x^2/2)$, which is maximized by $1/\sqrt{e}$ at $x = 1$. Since $\sqrt{2/\pi e} < 1$, the middle term is less than 1 and the derivative of the posterior odds under a flat prior for α, with respect to σ^2, is non-negative. The upper bound for σ^2 thus provides an upper bound on the posterior odds. We see that the posterior likelihood $\prod_i p_A(K_i|\bar{S}_i)$ increases from σ_L^2 to σ_U^2 (reflected in the log posterior odds ratio for the simplex volume vs the simplex area, Figs. 1-5a, b).

The derivative of the posterior odds under the Poisson Jeffreys prior, Eq. 29, with respect to σ^2, is proportional to

$$-\frac{\alpha^2}{2\sigma^3}\exp\left(-\frac{\alpha^2}{4\sigma^2}\right)\left(\mathcal{I}_{-\frac{5}{4}}\left(\frac{\alpha^2}{4\sigma^2}\right) + \mathcal{I}_{-\frac{3}{4}}\left(\frac{\alpha^2}{4\sigma^2}\right) + 2\mathcal{I}_{-\frac{1}{4}}\left(\frac{\alpha^2}{4\sigma^2}\right) + 2\mathcal{I}_{\frac{1}{4}}\left(\frac{\alpha^2}{4\sigma^2}\right) + \mathcal{I}_{\frac{3}{4}}\left(\frac{\alpha^2}{4\sigma^2}\right) + \mathcal{I}_{\frac{5}{4}}\left(\frac{\alpha^2}{4\sigma^2}\right)\right) \tag{54}$$

We saw that the posterior odds for the simplex area distribution also increased with σ^2 for the Poisson Jeffreys prior (Figs. 1-5d, e).

Zero-truncated binomial model

The marginal likelihood for the zero-truncated binomial with distribution p_B is

$$p_B(\{K_i\}) = \int dq\, p(q) \prod_i p_B(K_i|N,q) \approx \left(\prod_i p_B(K_i|N,\hat{q})\right) \int dq\, p(q) \prod_i \exp\left(-\frac{(q-\hat{q})^2}{2\sigma^2}\right) \tag{55}$$

where $p_B(K_i|N,q)$ is given by Eq. 11. For connections to larval KCs, we used the total number of traced projection neurons (PNs) and KCs as the binomial parameter N, averaged over the two sides of the brain [39]. For projections from larval KCs, we used the total number of KCs and output neurons, averaged over the two sides, as N. For projection to adult KCs, we used the number of Kenyon cells plus 150 (the estimated number of olfactory PNs) as N [60]. For projections from adult KCs, we used the number of KCs and output neurons labelled in the data as N.

The derivates of $\ln p_B$ are, again dropping indices on K,

$$\begin{aligned}\frac{\partial}{\partial q}\ln p_B &= \frac{K}{q} - \frac{N-K}{1-q} - \frac{N(1-q)^{N-1}}{1-(1-q)^N} \\ \frac{\partial^2}{\partial q^2}\ln p_B &= -\frac{K}{q^2} + \frac{N-K}{(1-q)^2} + \frac{N\left(N-1+(1-q)^N\right)(1-q)^{N-2}}{\left((1-q)^N-1\right)^2}\end{aligned} \tag{56}$$

The maximum likelihood parameter $\hat{q}$ for the zero-truncated binomial, with M samples of K, each with N trials, obeys:

$$\frac{\hat{q}}{1-(1-\hat{q})^N} = \frac{\sum_{i=1}^{M} K_i}{MN} \tag{57}$$

and the variance at $\hat{q}$ is

$$\sigma^2 = \left(\sum_i \left(\frac{K_i}{\hat{q}^2} - \frac{N-K_i}{(1-\hat{q})^2} - \frac{N\left(N-1+(1-\hat{q})^N\right)(1-\hat{q})^{N-2}}{\left((1-\hat{q})^N-1\right)^2} \right)^{-1} \right)^{-1} \tag{58}$$

Optimal degrees: bounded net weight

Now we examine what numbers of synaptic partners maximize the size of the allowed configuration space under the bounded net weight constraint. Here we generalize the constraint to allow the maximum total synaptic weight to explicitly depend on the number of inputs, K:

$$\sum_{i=1}^{K} J_i \leq \bar{J} K^p \tag{59}$$

This replaces the maximum weight $\bar{J}$ with $K^p \bar{J}$ in the volume:

$$V = \frac{(\bar{J}K^p)^K}{K!} \tag{60}$$

The volume is non-decreasing in $\bar{J}$. We compute its derivative with respect to K by analytically continuing the factorial to real values of K as the Gamma function, yielding

$$\begin{aligned} \frac{\partial V}{\partial K} &= \frac{(\bar{J}K^p)^K}{K!}\left(\ln \bar{J}K^p + p + \gamma - H_K\right) \\ &= \frac{(\bar{J}K^p)^K}{K!}\left(\ln \bar{J}K^p + p - \ln K - \frac{1}{2K} + \mathcal{O}\left(K^{-2}\right)\right) \end{aligned} \tag{61}$$

where H_X is the Xth harmonic number,

$$H_X = \sum_{x=1}^{X} \frac{1}{x} \tag{62}$$

We used Euler's expansion for the harmonic numbers,

$$H_X = \gamma + \ln X + \frac{1}{2X} + \mathcal{O}\left(X^{-2}\right) \tag{63}$$

At a critical point in K, truncating $\mathcal{O}(1/K^2)$ and higher-order terms, we find

$$\begin{aligned} \bar{J}(K^*)^p &= e^{\frac{1}{2K^*}-p}(K^*) + \mathcal{O}(1/K^2) \\ &= \left(K^* + \frac{1}{2}\right)\exp(-p) + \mathcal{O}(1/K^*) \end{aligned} \tag{64}$$

Substituting $K^p \bar{J} = \alpha \bar{S}$ yields

$$K^* = \alpha \exp(p)\bar{S} - \frac{1}{2} + \mathcal{O}(1/K^*) \tag{65}$$

Alternatively, the critical point can be calculated without first extending K to real numbers by using ratios:

$$1 = \frac{V(K^*)}{V(K^*+1)} = \frac{(K^*+1)^{1-p}}{\bar{J}} \left(\frac{K^*}{K^*+1}\right)^{pK^*} \tag{66}$$

which yields

$$\begin{aligned} \bar{J}(K^*)^p &= (K^*+1)\left(\frac{K^*}{K^*+1}\right)^{p(K^*+1)} \\ &= (K^*+1-p)\exp(-p) + \mathcal{O}(1/K^*) \end{aligned} \tag{67}$$

Optimal degrees: fixed net weight

If $\sum_j J_j = \bar{J}K^p$ then we have the surface area of the $K-1$ simplex. We consider a regular simplex (equal side lengths) with vertex length $\bar{J}K^p$ (from the origin to any vertex). Its surface area is

$$A = \frac{(\bar{J}K^p)^{K-1}\sqrt{K}}{(K-1)!} \tag{68}$$

By the same method as above, the derivative with respect to K is

$$\begin{aligned} \frac{\partial A}{\partial K} &= \frac{(\bar{J}K^p)^{K-1}}{2\sqrt{K}(K-1)!}\left(2K\ln(\bar{J}K^p) + 2(K-1)p - 2K(H_{K-1}-\gamma) + 1\right) \\ &= \frac{(\bar{J}K^p)^{K-1}}{2\sqrt{K}(K-1)!}\Bigg(2K\ln(\bar{J}K^p) + 2(K-1)p \\ &\quad - 2K\left(\ln(K-1) + \frac{1}{2(K-1)} + \mathcal{O}\left(\frac{1}{K^2}\right)\right) + 1\Bigg) \end{aligned} \tag{69}$$

Since H_{K-1} appears in the derivative, we only consider the derivative at $K \geq 2$. At a critical point in K, dividing through by K and truncating $\mathcal{O}(1/K^2)$ and higher-order terms yields

$$\begin{aligned} \ln \bar{J}K^p &= -p\frac{K-1}{K} + \ln(K-1) - \frac{1}{2K} - \frac{1}{2(K-1)} + \mathcal{O}(1/K^2) \\ \bar{J}K^p &= (K-1)\exp(-p)\exp\left(p/K - \frac{1}{2K} - \frac{1}{2(K-1)} + \mathcal{O}(1/K^2)\right) \\ &= \exp(-p)\,(K+p-2) + \mathcal{O}(1/K) \end{aligned} \tag{70}$$

and substituting $K^p\bar{J} = \alpha\bar{S}$ yields

$$K^* = \alpha\exp(p)\bar{S} + 2 - p + \mathcal{O}(1/K^*) \tag{71}$$

If we do not continue to real K first, we instead have

$$1 = \frac{A(K^*)}{A(K^*+1)} = \frac{(K^*)^{1-p}}{\bar{J}}\left(\frac{K^*}{K^*+1}\right)^{pK^*+\frac{1}{2}} \tag{72}$$

which yields

$$\begin{aligned} \bar{J}(K^*)^p &= K^*\left(\frac{K^*}{K^*+1}\right)^{pK^*+\frac{1}{2}} \\ &= \left(K^* + \frac{p-1}{2}\right)\exp(-p) + \mathcal{O}(1/K^*) \end{aligned} \tag{73}$$

Distances in synaptic configuration space

Above we assumed that synaptic weight configurations could travel between different points in the synaptic weight space along straight lines, endowing the K-dimensional synaptic weight space with a Euclidean (or 2-) norm. This amounts to assuming that synaptic weights can vary together. This could be interpreted, for example, as allowing a unit of synaptic weight (a receptor, perhaps) to be transferred directly between connections. An alternative is to assume that synaptic weights must move separately, which corresponds endowing the synaptic weight space with the 1-norm. In the above interpretation this would mean separating the removal of a receptor from one synapse from the addition of a receptor to another synapse. This changes the surface area of the simplex, since the length of that normal vector in computing it is now K instead of $\sqrt{K}$:

$$A_1 = \frac{(\bar{J}K^p)^{K-1}K}{(K-1)!} \tag{74}$$

Changing the norm for the synaptic weights leaves the above calculation of the posterior odds for the fixed net weight model mostly unchanged. The factors of $\sqrt{K}$ in the normalization constant are replaced by K; this removes the square roots in the derivation of the upper bound for the variance with respect to α so that

$$\frac{K-1}{\alpha^2} \leq \sigma^2 < \frac{K-1}{\alpha^2} + 2S^2 \tag{75}$$

The optimal number of connections can be calculated in the same manner as previously. The derivative of A_1 with respect to K is (to order $1/K$):

$$\frac{\partial A_1}{\partial K} \approx \frac{(\bar{J}K^p)^{K-1}}{(K-1)!}\left(K\ln\bar{J}K^p + (K-1)p - K\left(\ln(K-1) + \frac{1}{2(K-1)} + \mathcal{O}\left(\frac{1}{K^2}\right)\right) + 1\right) \tag{76}$$

At a critical point in K, truncating $\mathcal{O}(1/K^2)$ and higher-order terms yields

$$\bar{J} \approx K^{-p}(K-1)\exp\left(\frac{1}{K(K-1)} - p\frac{K-1}{K}\right) \tag{77}$$

Acknowledgments

We thank Ramakrishnan Iyer and Casey Schneider-Mizell for helpful discussions. We wish to thank the Allen Institute founder, Paul G. Allen, for his vision, encouragement and support.

Author contributions

Conceptualization: G.K.O and M.A.B. Formal analysis: G.K.O. Writing (original draft): G.K.O. Writing (review and editing): G.K.O and M.A.B. Supervision: M.A.B.

References

1. Laughlin S. A simple coding procedure enhances a neuron's information capacity. Zeitschrift Fur Naturforschung Section C, Biosciences. 1981;36(9-10):910–912.

2. Atick JJ, Redlich AN. Towards a Theory of Early Visual Processing. Neural Computation. 1990;2(3):308–320. doi:10.1162/neco.1990.2.3.308.

3. Bastos AM, Usrey WM, Adams RA, Mangun GR, Fries P, Friston KJ. Canonical Microcircuits for Predictive Coding. Neuron. 2012;76(4):695–711. doi:10.1016/j.neuron.2012.10.038.

4. Denève S, Machens CK. Efficient codes and balanced networks. Nature Neuroscience. 2016;19(3):375–382. doi:10.1038/nn.4243.

5. Chalk M, Marre O, Tkačik G. Toward a unified theory of efficient, predictive, and sparse coding. Proceedings of the National Academy of Sciences. 2017; p. 201711114. doi:10.1073/pnas.1711114115.

6. Albus JS. A theory of cerebellar function. Mathematical Biosciences. 1971;10(1):25–61. doi:10.1016/0025-5564(71)90051-4.

7. Marr D. A theory of cerebellar cortex. The Journal of Physiology. 1969;202(2):437–470.

8. Hopfield JJ. Neural networks and physical systems with emergent collective computational abilities. Proceedings of the National Academy of Sciences. 1982;79(8):2554–2558.

9. Barak O, Rigotti M, Fusi S. The sparseness of mixed selectivity neurons controls the generalization-discrimination trade-off. The Journal of Neuroscience: The Official Journal of the Society for Neuroscience. 2013;33(9):3844–3856. doi:10.1523/JNEUROSCI.2753-12.2013.

10. Rigotti M, Barak O, Warden MR, Wang XJ, Daw ND, Miller EK, et al. The importance of mixed selectivity in complex cognitive tasks. Nature. 2013;497(7451):585–590. doi:10.1038/nature12160.

11. Babadi B, Sompolinsky H. Sparseness and Expansion in Sensory Representations. Neuron. 2014;83(5):1213–1226. doi:10.1016/j.neuron.2014.07.035.

12. Litwin-Kumar A, Harris KD, Axel R, Sompolinsky H, Abbott LF. Optimal Degrees of Synaptic Connectivity. Neuron. 2017;93(5):1153–1164.e7. doi:10.1016/j.neuron.2017.01.030.

13. Brunel N, Hakim V, Isope P, Nadal JP, Barbour B. Optimal Information Storage and the Distribution of Synaptic Weights: Perceptron versus Purkinje Cell. Neuron. 2004;43(5):745–757. doi:10.1016/j.neuron.2004.08.023.

14. Chapeton J, Fares T, LaSota D, Stepanyants A. Efficient associative memory storage in cortical circuits of inhibitory and excitatory neurons. Proceedings of the National Academy of Sciences. 2012;109(51):E3614–E3622. doi:10.1073/pnas.1211467109.

15. Brunel N. Is cortical connectivity optimized for storing information? Nature Neuroscience. 2016;19(5):749–755. doi:10.1038/nn.4286.

16. Pereira U, Brunel N. Attractor Dynamics in Networks with Learning Rules Inferred from In Vivo Data. Neuron. 2018;99(1):227–238.e4. doi:10.1016/j.neuron.2018.05.038.

17. Durbin R, Mitchison G. A dimension reduction framework for understanding cortical maps. Nature. 1990;343(6259):644–647. doi:10.1038/343644a0.

18. Cherniak C. Component placement optimization in the brain. Journal of Neuroscience. 1994;14(4):2418–2427. doi:10.1523/JNEUROSCI.14-04-02418.1994.

19. Cherniak C, Mokhtarzada Z, Rodriguez-Esteban R, Changizi K. Global optimization of cerebral cortex layout. Proceedings of the National Academy of Sciences. 2004;101(4):1081–1086. doi:10.1073/pnas.0305212101.

20. Weigand M, Sartori F, Cuntz H. Universal transition from unstructured to structured neural maps. Proceedings of the National Academy of Sciences. 2017;114(20):E4057–E4064. doi:10.1073/pnas.1616163114.

21. Bullmore E, Sporns O. The economy of brain network organization. Nature Reviews Neuroscience. 2012;13(5):336–349. doi:10.1038/nrn3214.

22. Cuntz H, Forstner F, Borst A, Häusser M. One Rule to Grow Them All: A General Theory of Neuronal Branching and Its Practical Application. PLOS Computational Biology. 2010;6(8):e1000877. doi:10.1371/journal.pcbi.1000877.

23. Cuntz H, Mathy A, Häusser M. A scaling law derived from optimal dendritic wiring. Proceedings of the National Academy of Sciences of the United States of America. 2012;109(27):11014–11018. doi:10.1073/pnas.1200430109.

24. Kasai H, Matsuzaki M, Noguchi J, Yasumatsu N, Nakahara H. Structure-stability-function relationships of dendritic spines. Trends in Neurosciences. 2003;26(7):360–368. doi:10.1016/S0166-2236(03)00162-0.

25. Turrigiano GG, Leslie KR, Desai NS, Rutherford LC, Nelson SB. Activity-dependent scaling of quantal amplitude in neocortical neurons. Nature. 1998;361:892–896.

26. Desai NS, Cudmore RH, Nelson SB, Turrigiano GG. Critical periods for experience-dependent synaptic scaling in visual cortex. Nature Neuroscience. 2002;5(8):783–789. doi:10.1038/nn878.

27. Goel A, Jiang B, Xu LW, Song L, Kirkwood A, Lee HK. Cross-modal regulation of synaptic AMPA receptors in primary sensory cortices by visual experience. Nature Neuroscience. 2006;9(8):1001–1003. doi:10.1038/nn1725.

28. Goold CP, Nicoll RA. Single-Cell Optogenetic Excitation Drives Homeostatic Synaptic Depression. Neuron. 2010;68(3):512–528. doi:10.1016/j.neuron.2010.09.020.

29. Vale C, Sanes DH. The effect of bilateral deafness on excitatory and inhibitory synaptic strength in the inferior colliculus. European Journal of Neuroscience. 2002;16(12):2394–2404. doi:10.1046/j.1460-9568.2002.02302.x.

30. Hartman KN, Pal SK, Burrone J, Murthy VN. Activity-dependent regulation of inhibitory synaptic transmission in hippocampal neurons. Nature Neuroscience. 2006;9(5):642–649. doi:10.1038/nn1677.

31. Joseph A, Turrigiano GG. All for One But Not One for All: Excitatory Synaptic Scaling and Intrinsic Excitability Are Coregulated by CaMKIV, Whereas Inhibitory Synaptic Scaling Is Under Independent Control. The Journal of Neuroscience: The Official Journal of the Society for Neuroscience. 2017;37(28):6778–6785. doi:10.1523/JNEUROSCI.0618-17.2017.

32. Maffei A, Nelson SB, Turrigiano GG. Selective reconfiguration of layer 4 visual cortical circuitry by visual deprivation. Nature Neuroscience. 2004;7(12):1353–1359. doi:10.1038/nn1351.

33. Kilman V, Rossum MCWv, Turrigiano GG. Activity Deprivation Reduces Miniature IPSC Amplitude by Decreasing the Number of Postsynaptic GABAA Receptors Clustered at Neocortical Synapses. Journal of Neuroscience. 2002;22(4):1328–1337. doi:10.1523/JNEUROSCI.22-04-01328.2002.

34. Hengen KB, Lambo ME, Van Hooser SD, Katz DB, Turrigiano GG. Firing rate homeostasis in visual cortex of freely behaving rodents. Neuron. 2013;80(2):335–342. doi:10.1016/j.neuron.2013.08.038.

35. Grueber WB, Jan LY, Jan YN. Tiling of the Drosophila epidermis by multidendritic sensory neurons. Development (Cambridge, England). 2002;129(12):2867–2878.

36. Keshishian H, Chiba A, Chang TN, Halfon MS, Harkins EW, Jarecki J, et al. Cellular mechanisms governing synaptic development in Drosophila melanogaster. Journal of Neurobiology. 1993;24(6):757–787. doi:10.1002/neu.480240606.

37. Gerhard S, Andrade I, Fetter RD, Cardona A, Schneider-Mizell CM. Conserved neural circuit structure across Drosophila larval development revealed by comparative connectomics. eLife. 2017;6:e29089. doi:10.7554/eLife.29089.

38. Tripodi M, Evers JF, Mauss A, Bate M, Landgraf M. Structural Homeostasis: Compensatory Adjustments of Dendritic Arbor Geometry in Response to Variations of Synaptic Input. PLOS Biology. 2008;6(10):e260. doi:10.1371/journal.pbio.0060260.

39. Eichler K, Li F, Litwin-Kumar A, Park Y, Andrade I, Schneider-Mizell CM, et al. The complete connectome of a learning and memory centre in an insect brain. Nature. 2017;548(7666):175–182. doi:10.1038/nature23455.

40. Takemura Sy, Aso Y, Hige T, Wong A, Lu Z, Xu CS, et al. A connectome of a learning and memory center in the adult Drosophila brain. eLife. 2017;6:e26975. doi:10.7554/eLife.26975.

41. Murthy M, Fiete I, Laurent G. Testing odor response stereotypy in the Drosophila mushroom body. Neuron. 2008;59(6):1009–1023. doi:10.1016/j.neuron.2008.07.040.

42. Caron SJC, Ruta V, Abbott LF, Axel R. Random convergence of olfactory inputs in the *Drosophila* mushroom body. Nature. 2013;497(7447):113–117. doi:10.1038/nature12063.

43. Stevens CF. What the fly's nose tells the fly's brain. Proceedings of the National Academy of Sciences. 2015;112(30):9460–9465. doi:10.1073/pnas.1510103112.

44. Heisenberg M. Mushroom body memoir: from maps to models. Nature Reviews Neuroscience. 2003;4(4):266–275. doi:10.1038/nrn1074.

45. Srinivasan S, Greenspan RJ, Stevens CF, Grover D. Deep(er) Learning. Journal of Neuroscience. 2018;38(34):7365–7374. doi:10.1523/JNEUROSCI.0153-18.2018.

46. Turrigiano GG. The Self-Tuning Neuron: Synaptic Scaling of Excitatory Synapses. Cell. 2008;135(3):422–435. doi:10.1016/j.cell.2008.10.008.

47. Owald D, Waddell S. Olfactory learning skews mushroom body output pathways to steer behavioral choice in Drosophila. Current Opinion in Neurobiology. 2015;35:178–184. doi:10.1016/j.conb.2015.10.002.

48. Masuda-Nakagawa LM, Tanaka NK, O'Kane CJ. Stereotypic and random patterns of connectivity in the larval mushroom body calyx of Drosophila. Proceedings of the National Academy of Sciences of the United States of America. 2005;102(52):19027–19032. doi:10.1073/pnas.0509643102.

49. Zhu S, Chiang AS, Lee T. Development of the Drosophila mushroom bodies: elaboration, remodeling and spatial organization of dendrites in the calyx. Development (Cambridge, England). 2003;130(12):2603–2610. doi:10.1242/dev.00466.

50. Lin HH, Lai JSY, Chin AL, Chen YC, Chiang AS. A Map of Olfactory Representation in the Drosophila Mushroom Body. Cell. 2007;128(6):1205–1217. doi:10.1016/j.cell.2007.03.006.

51. Harris KM, Stevens JK. Dendritic spines of CA 1 pyramidal cells in the rat hippocampus: serial electron microscopy with reference to their biophysical characteristics. The Journal of Neuroscience: The Official Journal of the Society for Neuroscience. 1989;9(8):2982–2997.

52. Harris KM, Sultan P. Variation in the number, location and size of synaptic vesicles provides an anatomical basis for the nonuniform probability of release at hippocampal CA1 synapses. Neuropharmacology. 1995;34(11):1387–1395.

53. Schikorski T, Stevens CF. Quantitative Ultrastructural Analysis of Hippocampal Excitatory Synapses. Journal of Neuroscience. 1997;17(15):5858–5867. doi:10.1523/JNEUROSCI.17-15-05858.1997.

54. Schikorski T, Stevens CF. Morphological correlates of functionally defined synaptic vesicle populations. Nature Neuroscience. 2001;4(4):391–395. doi:10.1038/86042.

55. Bourne JN, Chirillo MA, Harris KM. Presynaptic ultrastructural plasticity along CA3→CA1 axons during long-term potentiation in mature hippocampus. The Journal of Comparative Neurology. 2013;521(17):3898–3912. doi:10.1002/cne.23384.

56. Jeffreys Harold. An invariant form for the prior probability in estimation problems. Proceedings of the Royal Society of London Series A Mathematical and Physical Sciences. 1946;186(1007):453–461. doi:10.1098/rspa.1946.0056.

57. van Vreeswijk C, Sompolinsky H. Chaos in neuronal networks with balanced excitatory and inhibitory activity. Science (New York, NY). 1996;274(5293):1724–1726.

58. Gardner E. The space of interactions in neural network models. Journal of Physics A: Mathematical and General. 1988;21(1):257. doi:10.1088/0305-4470/21/1/030.

59. Chapeton J, Gala R, Stepanyants A. Effects of homeostatic constraints on associative memory storage and synaptic connectivity of cortical circuits. Frontiers in Computational Neuroscience. 2015;9. doi:10.3389/fncom.2015.00074.

60. Jefferis GS, Marin EC, Stocker RF, Luo L. Target neuron prespecification in the olfactory map of Drosophila. Nature. 2001;414(6860):204–208. doi:10.1038/35102574.

Supporting Figures

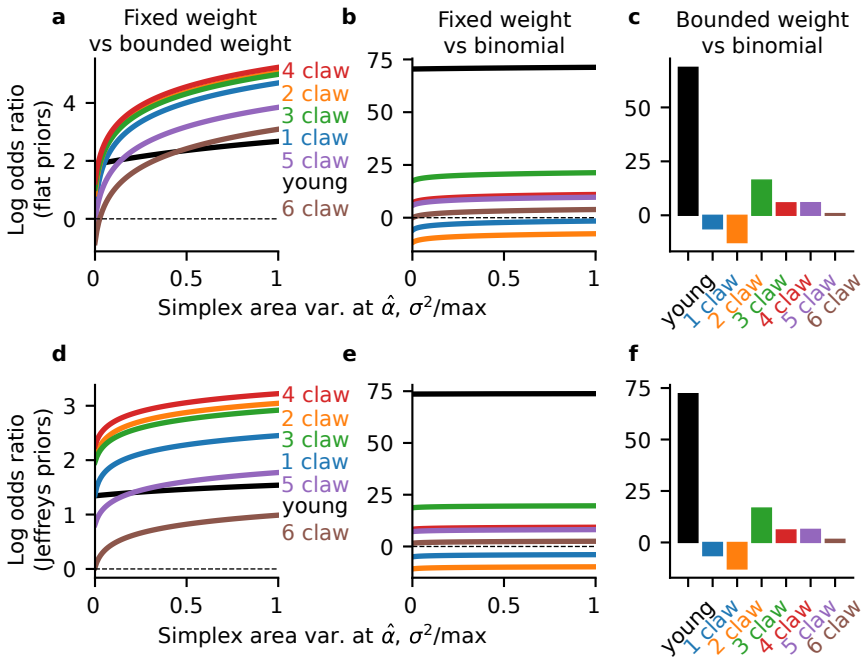

Supp. Fig. 1. Log odds ratios for larval Kenyon cell input degrees. (**a**) Log posterior odds ratio for the simplex area distribution vs the simplex volume distribution, under a flat prior for the parameter α. All posterior odds are computed by the Laplace approximation—a gaussian approximation for the likelihood in α. The Laplace approximation yields point estimates of the posterior odds for the simplex volume and zero-truncated binomial models (Methods: ,). For the simplex area model, this yields lower and upper bounds for the posterior odds (Methods:). Those bounds are parameterized by the variance of that gaussian, σ_α^2. For each cell type, we varied σ_α^2 between its lower and upper bounds and computed the posterior odds at each σ_α^2. Since those bounds differ between cell types, we normalized them to compare the odds ratios. (**b**) Same as a), for the simplex area vs the zero-truncated binomial model. (**c**) Posterior odds ratio for the simplex volume vs the zero-truncated binomial model. (**d-f**) Same as (a-c), but with the Poisson Jeffreys prior for α, $p(\alpha) \propto 1/\sqrt{\sigma}$.

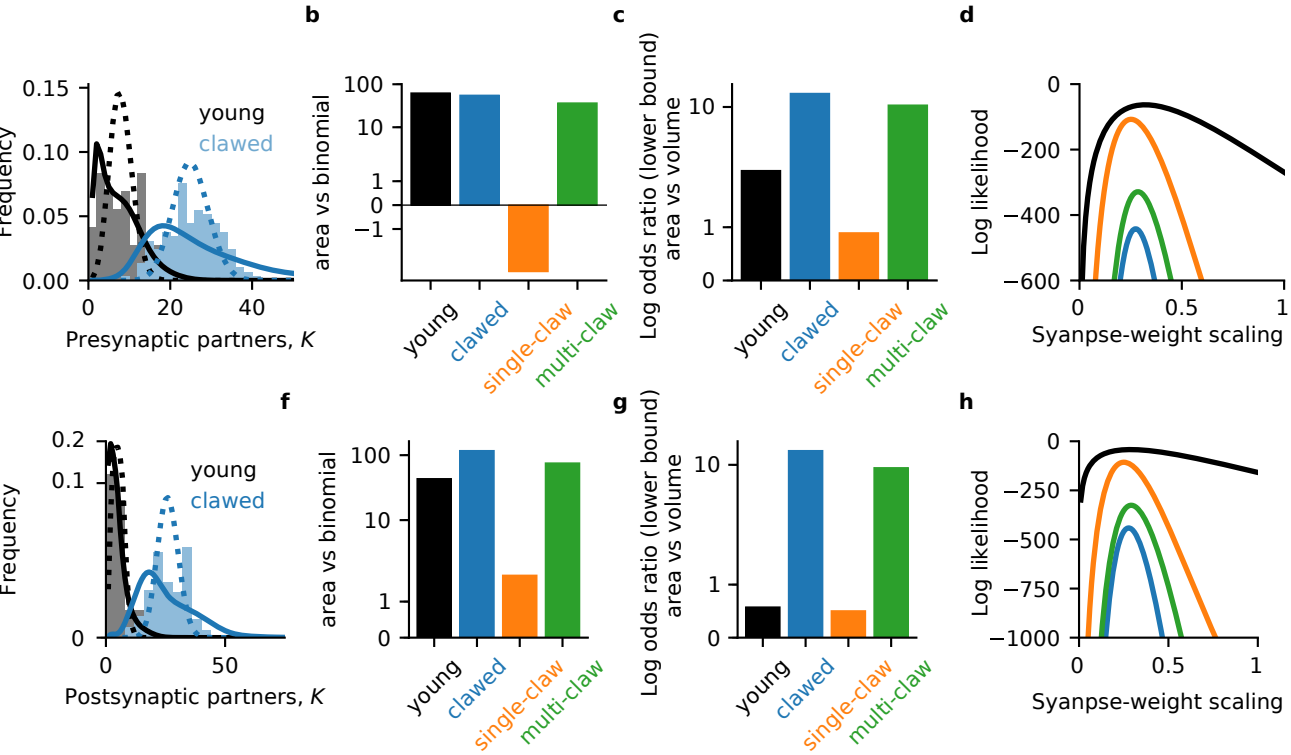

rval Kenyon cell axo-axonal connectivity. (**a**) Input degree distributions for larval KCs. (**b**) Log odds ratio for the fixed net binomial wiring model. (**c**) Log odds ratio for the fixed net weight model vs bounded net weight model. (**d**) Likelihood as a pse-weight scaling parameter α. **e-h**) Same as (**a-d**) for KC axo-axonal outputs.

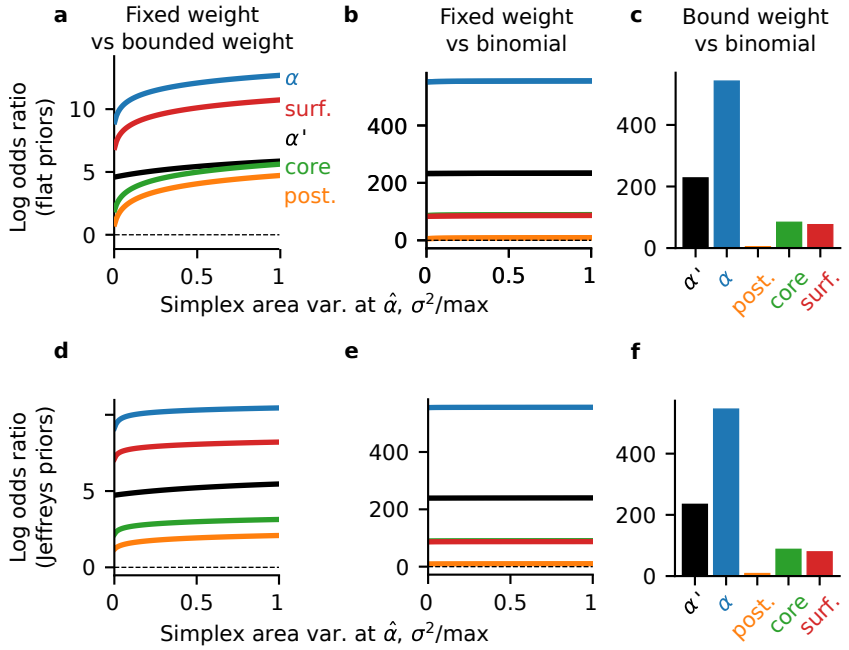

Supp. Fig. 3. Log odds ratios for adult Kenyon cell input degrees. Same as Supp. Fig. 1, but for adult Kenyon cells.

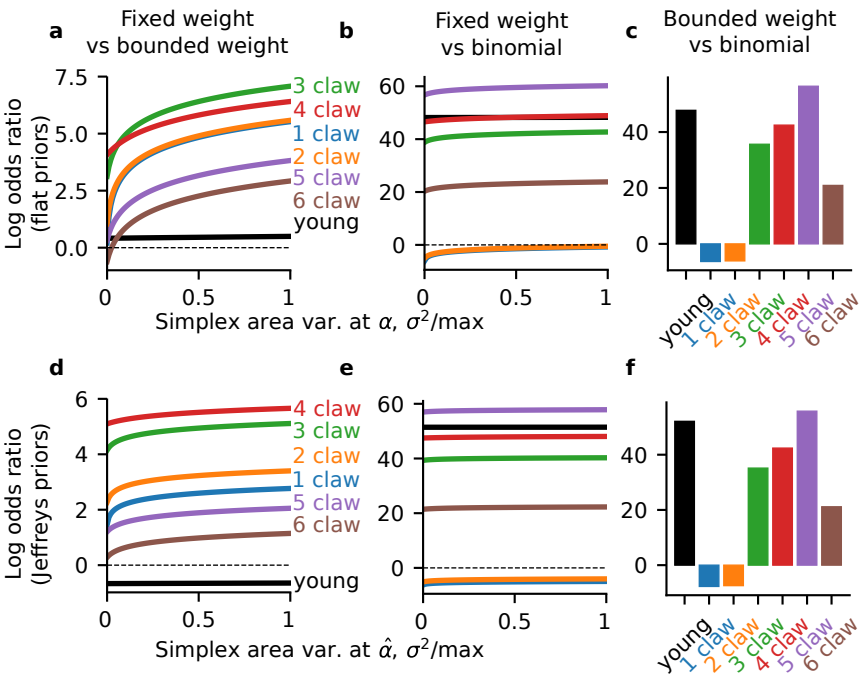

Supp. Fig. 4. Log odds ratios for larval Kenyon cell output degrees. Same as Supp. Fig. 1, but for larval Kenyon cell outputs.

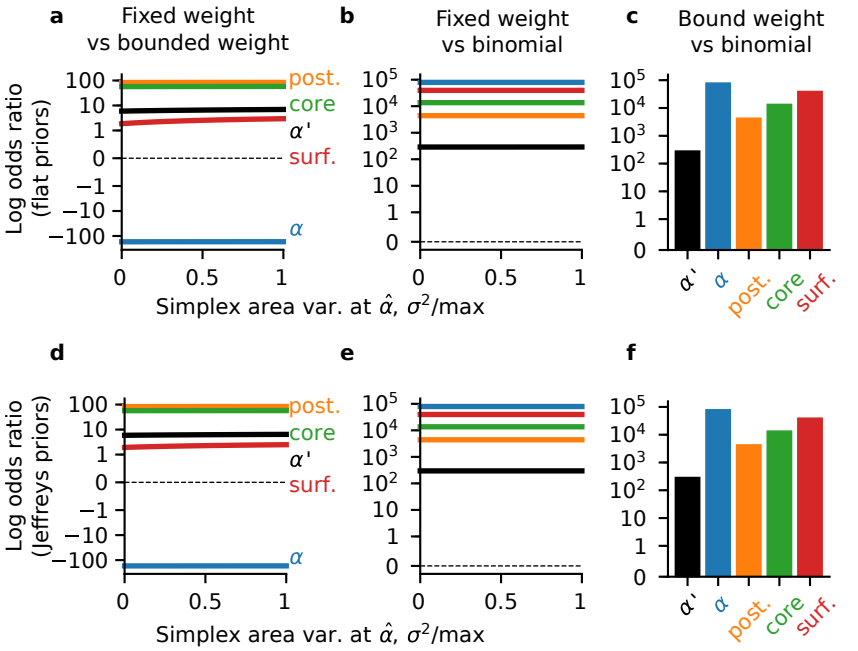

Supp. Fig. 5. Log odds ratios for adult Kenyon cell output degrees. Same as Supp. Fig. 1, but for adult Kenyon cell outputs.

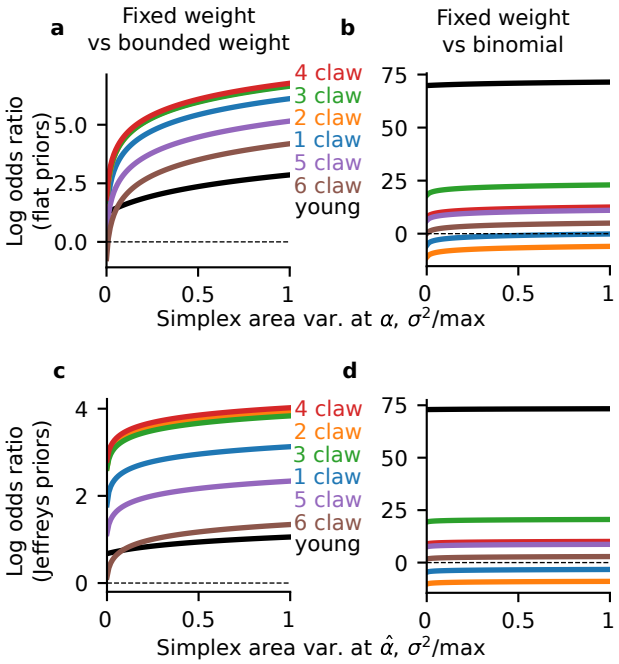

Supp. Fig. 6. Log odds ratios for larva Kenyon cell input degrees with 1-norm surface area model. Same as Supp. Fig. 1, but for the 1-norm simplex surface area model (Methods:).

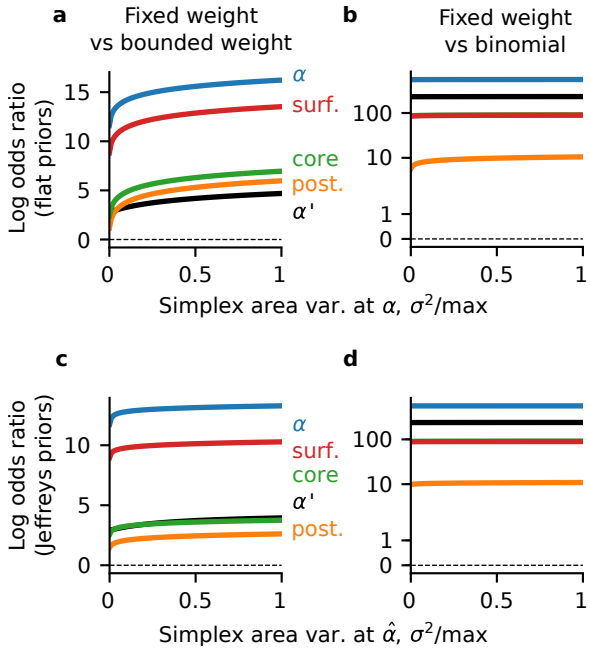

Supp. Fig. 7. Log odds ratios for adult Kenyon cell input degrees with 1-norm surface area model. Same as Supp. Fig. 3, but for the 1-norm simplex surface area model (Methods:).

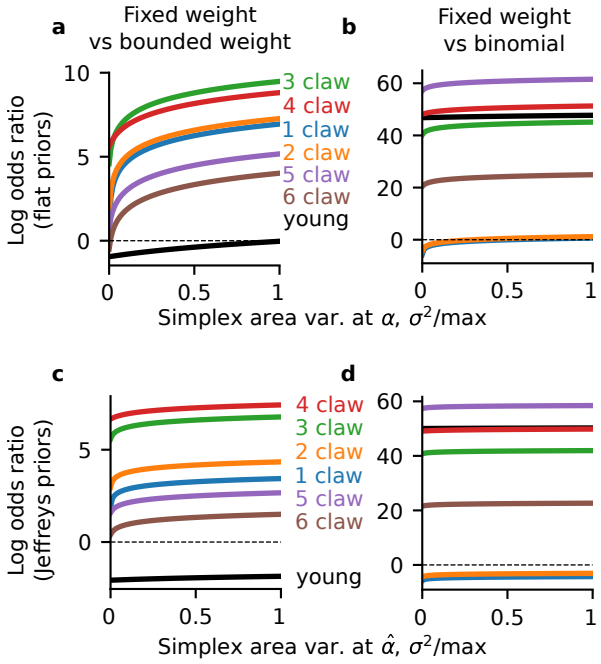

Supp. Fig. 8. Log odds ratios for larva Kenyon cell output degrees with 1-norm surface area model. Same as Supp. Fig. 4, but for the 1-norm simplex surface area model (Methods:).

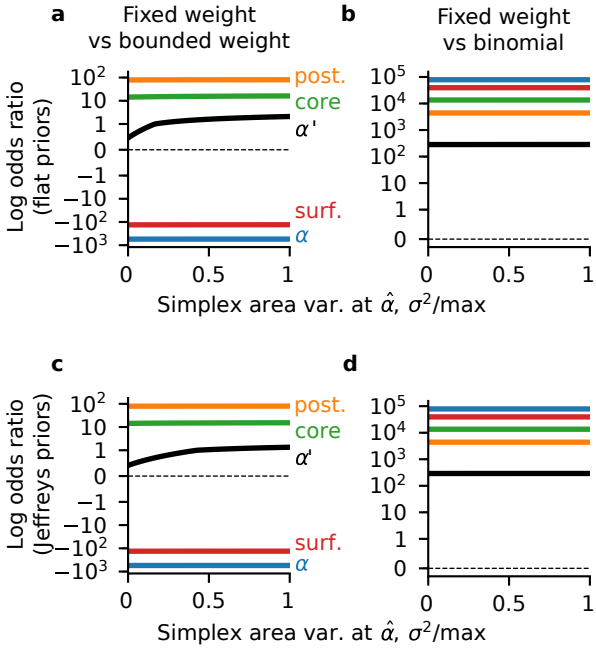

Supp. Fig. 9. Log odds ratios for adult Kenyon cell output degrees with 1-norm surface area model. Same as Supp. Fig. 5, but for the 1-norm simplex surface area model (Methods:).